

SIMULINK MODELLING OF RADON AND WAVELET TRANSFORMS FOR IMAGE FEATURE EXTRACTION

A. Gavlasová, A. Procházka

Institute of Chemical Technology, Department of Computing and Control Engineering

Abstract

Image analysis, de-noising, segmentation, feature extraction and classification form very important research topics of image processing. The paper is devoted to the rotation and translation invariant image transforms analysis and their use for image enhancement and features extraction. A special attention is paid to the two-dimensional Radon and wavelet transforms forming fundamental mathematical tools in these areas. Results are verified in the Simulink environment both for simulated data and for analysis of magnetic resonance biomedical images.

1 Introduction

The paper is devoted to the designing and creating of systems in the Simulink environment. These systems allow features extraction by blocks of Radon transform, wavelet transform and blocks of image preprocessing. Individual features are obtained by connection of these blocks using a wavelet decomposition block into the second level. Two features obtained by this decomposition are sum of squared image component coefficients evaluated in the first and the second decomposition level by high-pass filters both for image columns and rows. Results of features' variance with application of different methods are displayed both graphically and in the tables.

2 Basic Properties and Implementation of Radon Transform

Radon transform forming a very important mathematical tool used in tomography is based upon works of Johann Radon born in 1887 Litoměřice. His doctoral dissertation has been defended in Vienna in 1910 and his most appreciated works were devoted to integral geometry. The Radon transform [1] belonging to this category introduced in 1917 is defined as a collection of 1D projections around an object at angle intervals Θ . The Radon transform of a two-dimensional (2-D) function $f(x, y)$ is defined as

$$R(\Theta, r)[f(x, y)] = \int_{-\infty}^{+\infty} \int_{-\infty}^{+\infty} f(x, y) \delta(r - x \cos \Theta - y \sin \Theta) dx dy \quad (1)$$

where r is the perpendicular distance of a line from the origin and Θ is the angle formed by the distance vector.

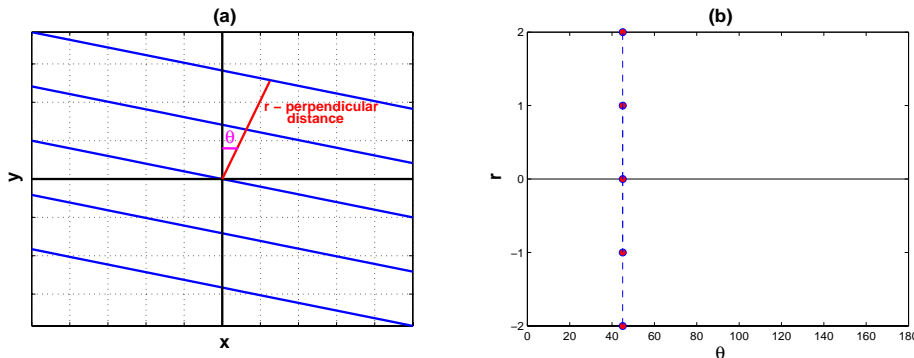


Figure 1: Figure presents (a) an example of a set of parallel lines for a chosen $\Theta = 45^\circ$ in the (x, y) plane and (b) the localization of corresponding points in the (Θ, r) plane in which the discrete Radon transform is evaluated

For the constant value of Θ the set of parallel lines for different values of r are presented in Fig. 1(a). The parallel lines are used for the integration of the given image. The plane (x, y) is transformed in this way to the plane (Θ, r) . The transformation proceeds by integration of the given image along parallel lines in the plane (x, y) and resulting value is then marked in the graph as a point for a given Θ and r as depicted in Fig. 1(b). Each point has a different intensity of color, depending on its value, having value 0 corresponding to black and 1 corresponding to white color presented in Fig. 3(b).

A discrete Radon transform called Hough transform has been introduced in 1972 by R. Duda and P. Hart [3] as a tool for image features extraction.

2.1 Simulation of Radon Transform in Simulink Environment

In the Simulink environment there is no block for the Radon transform. A general block called "Matlab function" can be used instead. This block has a single input and single output. Parameters of this block include:

- name of existing function of Matlab library or name of the created function as M-file
- output dimensions specified for returned single value
- choice to Collapse 2-D results to 1-D

The Matlab function or M-file use every "Matlab function" block for processing of the input value. Fig. 2 presents block diagram of the direct and inverse Radon transform of MR image and visualization of Radon transform image. Input image is loaded as a constant and output variable is frame-based. Input image and images after transformation are visualized in the matrix viewer presented in Fig. 3 and sent to workspace.

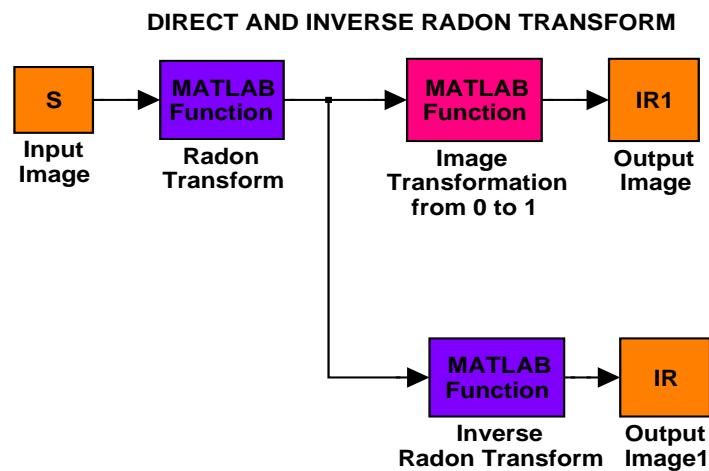


Figure 2: Block diagram of the proposed technique

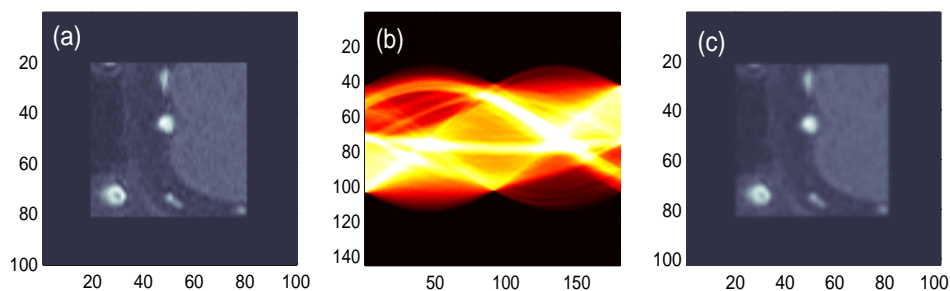


Figure 3: Visualization of (a) input MR image rotated by $\Theta = 90^\circ$, its (b) Radon transform depicted as points for $\Theta = 0^\circ - 180^\circ$ and for the same r for each Θ , and (c) inverse Radon transform

3 Principles of Image Wavelet Decomposition

Wavelet functions used for signal analysis are derived from the initial function $W(t)$ forming basis for the set of functions

$$W_{a,b}(t) = \frac{1}{\sqrt{a}} W\left(\frac{1}{a}(t-b)\right) \quad (2)$$

for discrete parameters of dilation $a = 2^m$ and translation $b = k 2^m$. Wavelet dilation, which is closely related to spectrum compression, enables local and global signal analysis. The principle of signal and image decomposition and reconstruction for resolution enhancement is presented in Fig. 4.

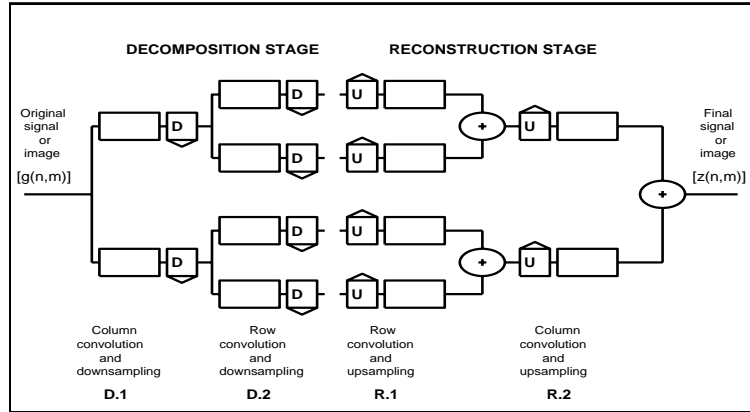


Figure 4: Mallat diagram for image decomposition and reconstruction

The decomposition stage results in this way in four images representing all combinations of low-pass and high-pass initial image matrix. The reconstruction stage includes row upsampling at first and row convolution in stage $R.1$. The corresponding images are then summed. The final step $R.2$ assumes column upsampling and convolution with reconstruction filters followed by summation of the results again. In the case of one-dimensional signal processing, steps $D.2$ and $R.1$ are omitted.

3.1 Simulation of Wavelet Transform in Simulink Environment

Wavelet transform diagram was created with blocks of Simulink library. Block "DWT" computes the discrete wavelet transform using a filter bank with specified highpass and lowpass filters. The filters can be user-defined or formed by wavelets of the Wavelet Toolbox. The output is set to 'Multiple ports'. It enables to see each subband as a frame-based vector or matrix. The common block "Transpose" enables matrix transposition. In our diagram it enables matrix transposition after column downsampling to proceed row decomposition. We transpose matrix after the row decomposition to visualize matrix right. Diagram for one decomposition and reconstruction levels is presented in Fig. 5.

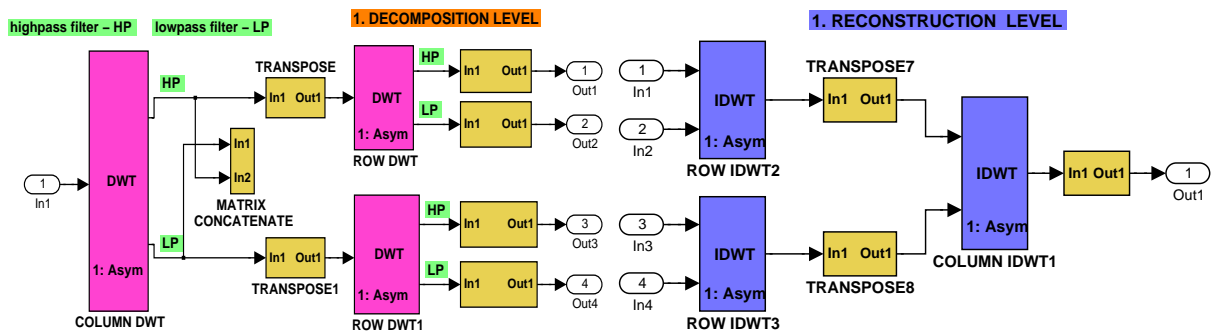


Figure 5: Figure presents connection of individual Simulink blocks which create one level of wavelet decomposition and reconstruction

The whole diagram for image decomposition into the second level and its reconstruction is presented in Fig. 6.

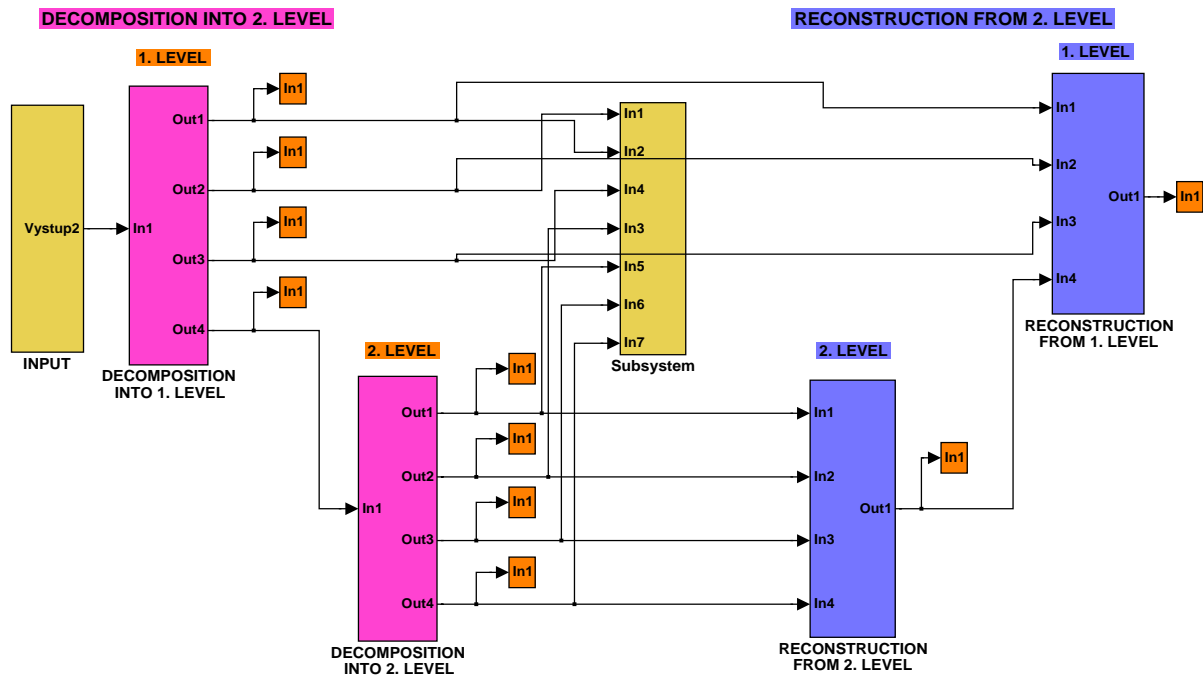


Figure 6: The simulink diagram for wavelet transform decomposition and reconstruction applied to two levels

Diagram was applied to a MR image. Resulting images from the matrix viewer are depicted in Fig. 7.

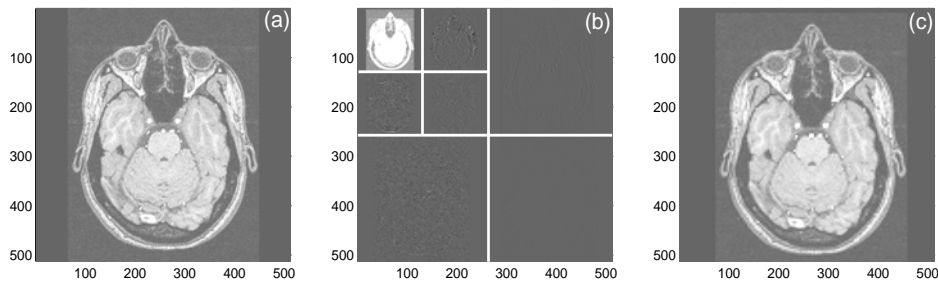


Figure 7: Visualization of (a) input MR image, its (b) wavelet decomposition, and (c) image wavelet reconstruction

Block diagrams mentioned above have been created to obtain definition of features of rotated images. We compare the standard deviation (STD) of the sum of squared diagonal DWT transform coefficients in the first and the second decomposition levels using MR images obtained by rotation from 0 to 180 degrees with step 10° using (i) diagram with the plain DWT, (ii) diagram for the Radon transform (RT) followed by the DWT diagram. Computed values of STD are displayed in Tab. 1.

Table 1: TABLE PRESENTS STD COMPUTED FROM ROTATED MR IMAGE FEATURES

STD of MR Image Features		
	Feature-1	Feature-2
DWT	0.0013	0.0254
RT-DWT	$2.97 \cdot 10^{-5}$	0.0023

4 Application to Image De-noising

The last step for image features extraction is based upon the connection of blocks for Image preprocessing, followed by Radon transform and Discrete wavelet transform application. Diagram of Image preprocessing presented in Fig. 8 enables image enhancement using thresholding. For thresholding we compute or select level of threshold, according to whose we can modify wavelet coefficients. They arise after wavelet decomposition into the selected level by using at least one highpass filter. In the Simulink environment a chosen threshold is applied through the block called "Dead zone". Output is zero for inputs within the dead zone.

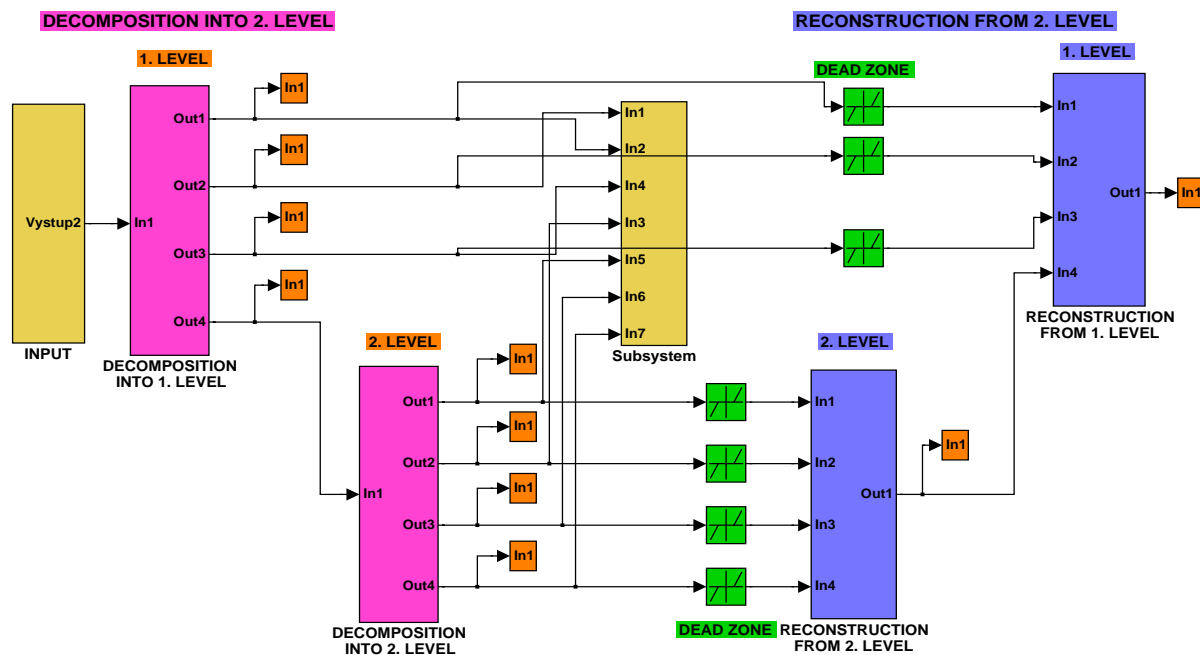


Figure 8: Simulink diagram for Image preprocessing using wavelet transform decomposition, dead zones for modification of wavelet coefficients and reconstruction applied to two levels

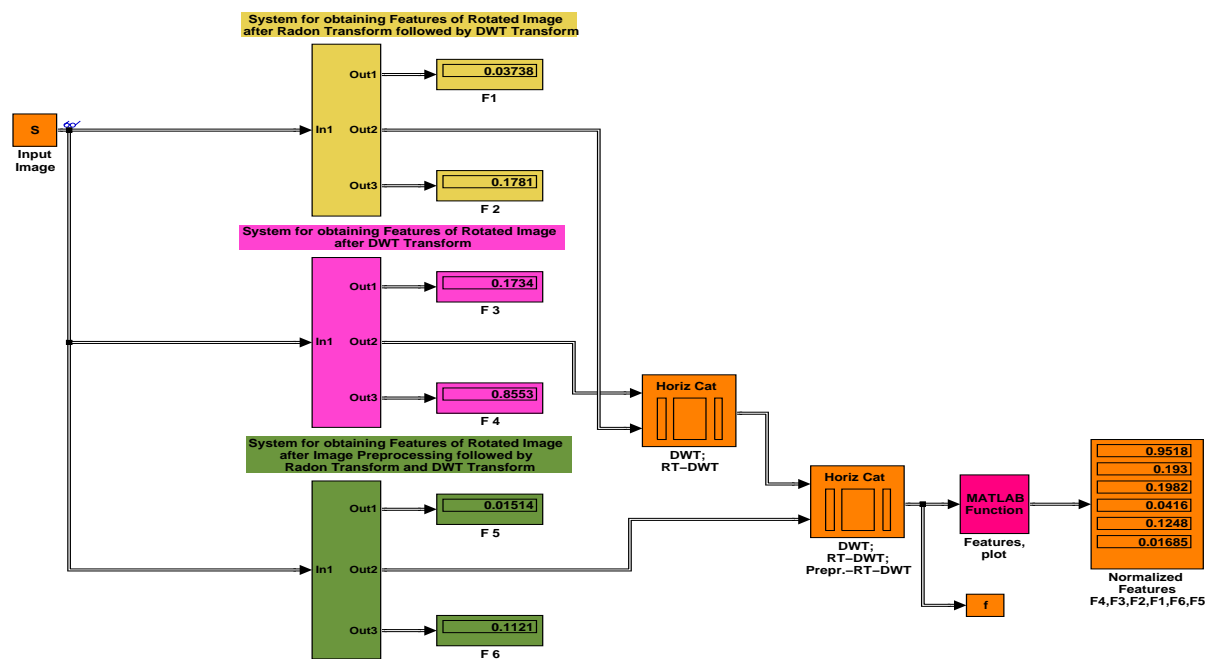


Figure 9: Image features extraction using proposed methods

Fig. 9 presents the whole diagram of three connected proposed methods. This diagram allows rotated image features extraction by using all the proposed methods. Process of image

rotation and features extraction in each step is visualized and resulting features are in each step depicted in a graph. Results of computed STD are presented in Tab. 2 and compared.

Table 2: COMPARISON OF STANDARD DEVIATION (STD) OF THE SUM OF SQUARED DIAGONAL DWT TRANSFORM COEFFICIENTS IN THE FIRST AND THE SECOND DECOMPOSITION LEVELS USING IMAGES OBTAINED BY ROTATION FROM 0 TO 180 DEGREES WITH STEP 10° USING (I) THE PLAIN DWT, (II) THE RADON TRANSFORM (RT) FOLLOWED BY DWT, AND (III) THE RT APPLIED TO THE PREPROCESSED A IMAGE (PRE) FOLLOWED BY THE DWT

STD of MR Image Features		
	Feature-1	Feature-2
DWT	0.0013	0.0254
RT-DWT	$2.97 \cdot 10^{-5}$	0.0023
Pre-RT-DWT	$1.4 \cdot 10^{-5}$	0.0016

5 Results

Thanks to the objective confrontation of STDs, Tab. 2 is the bright example that the Radon transform is a powerful tool expressively contributing to image analysis. The improvement of the STD between the plain DWT and RT-DWT by an order has been verified. We achieved also a small improvement by denoising of the magnetic resonance image. Therefore image enhancement is very desirable here. Image preprocessing allows further research devoted to the optimization of wavelet coefficients thresholding to denoise the original image.

Apparently in Fig. 10 the recommended connection of Radon and wavelet transforms dramatically keep down the features variance influenced by image rotation. If we moreover add the image preprocessing results are even better visible. Together with the visual comparison the concrete numerical results obtained point to the efficiency of the proposed method as presented in Tab. 2.

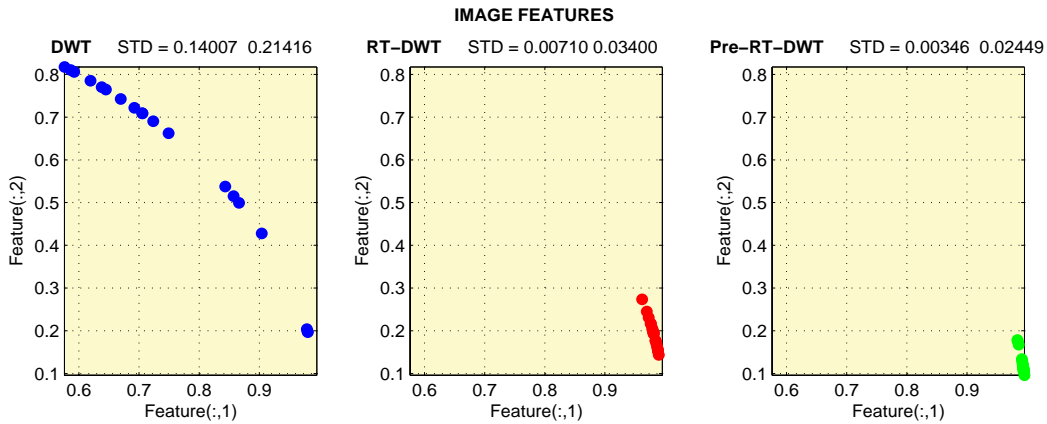


Figure 10: Results of feature extraction methods applied to real MR image obtained by image rotation from 0° to 180° with step 10°

Feature values presented in Fig. 10 are normalized to the unit circle to have a better comparison of clusters of image features and to allow their subsequent classification by self-organizing neural networks [2] into the given number of classes.

The proposed method of image features extraction allows the estimation of the rotation invariant image features and moreover it is very flexible as it allows the use of different wavelet functions and different rotation steps in case of the Radon transform. It is assumed that further studies will be devoted to feature based image segmentation and further methods of rotation and translation invariant feature selection using appropriate image transforms.

Acknowledgments

The work has been supported by the research grant of the Faculty of Chemical Engineering of the Institute of Chemical Technology, Prague No. MSM 6046137306.

References

- [1] R. N. Bracewell. *Fourier Analysis and Imaging*. Kluwer Academic Press, 2003.
- [2] D. I. Choi and S. H. Park. Self-Creating and Organizing Neural Networks. *IEEE Trans. Neural Networks*, 5(4):561–575, July 1994.
- [3] R. O. Duda and P. E. Hart. Use of the Hough Transformation to Detect Lines and Curves in Pictures. *Comm. ACM*, 15(1):11–15, 1972.

Ing. Andrea Gavlasová, Prof. Aleš Procházka
Institute of Chemical Technology, Prague
Department of Computing and Control Engineering
Technická 1905, 166 28 Prague 6 Phone: 00420-220 442 970, 00420-220 444 198
E-mail: Andrea.Gavlasova@vscht.cz, A.Prochazka@ieee.org